PHYSICAL REVIEW B VOLUME 15, NUMBER 4 15 FEBRUARY 1977

Band-population interference phenomena in the electroreflectance of narrow-gap semiconductors under heavy surface accumulation

N. Bottka
Michelson Laboratories, Naval Weapons Center, China Lake, California 93555

D. L. Johnson*
Ames Laboratory, United States Energy Research Development Administration, Iowa State University, Ames, Iowa 50011

R. Glosser
Physics Programs, University of Texas at Dallas, Richardson, Texas 75080
(Received 19 July 1976)

Band-population effects have been well established as being responsible for portions of the electroreflectance spectrum, in a metal-oxide-semiconductor configuration, of narrow-gap semiconductors. In this paper we show both experimentally and theoretically that these effects lead to unexpectedly strong interference phenomena and broadening under accumulation conditions at the surface. Specifically, as the gate bias is increased into accumulation the electroreflectance signal splits into two structures one of which shifts to the blue with increasing bias; the other is relatively insensitive to bias. The results can be directly correlated with the amount of surface band bending, the screening length, the bulk Fermi level, and band nonparabolicity. A simple oscillator model is used to describe the changes in the complex dielectric function. This model, when used with the Aspnes-Frova relation for spatially varying dielectrics, shows more clearly the origin of the observed phenomenon. This analysis facilitates the interpretation of electroreflectance data in degenerate semiconductors and allows determination of surface-related parameters.

I. INTRODUCTION

Band population in semiconductor materials occurs when, under steady-state conditions, the Fermi level E_F lies within the conduction- or valence-band states. This condition can occur either in the bulk of the material for heavy extrinsic doping or near its surface under heavy accumulation or inversion biasing. In either case, the band-population phenomenon manifests itself in optical measurements either as a shift in the fundamental absorption edge of the material as a function of doping (the Burstein-Moss shift[1,2]) or as a shift in the spectral position of electroreflectance (ER) structure as a function of applied voltages. In the latter case, this shift can be induced externally even in non- or near-degenerate materials by biasing the surface into heavy accumulation.[3,4]

Electroreflectance experiments indicate, however, that in addition to this spectral shift there is considerable broadening and sometimes even splitting (see below) in the observed structure under increased surface accumulation. At first this broadening and splitting was thought to reflect the band splittings at low-symmetry points in the Brillouin zone.[5] By considering the nonparabolicity of the bands involved in the transition it was concluded that these band splittings are far too small to explain the much larger observed broadening and splitting seen in ER of InSb and InAs.

It is the intent of this paper to focus on these phenomena and to show that they can be directly correlated with the amount of surface band bending, the screening length, the bulk Fermi level, and the band nonparabolicity. Furthermore, criteria are established for using ER to determine these quantities optically.

In Sec. II we present the experimental ER results for InSb and InAs showing band-population-induced broadening and splitting, respectively. Using relations described in the Appendices and the general formalism of Ref. 4 we describe the procedure for calculating the surface potential and the screening length for a degenerate semiconductor having a nonparabolic conduction band. Having established the spatial dependence of the potential, and thus the band population within the space-charge region, we proceed to calculate the change in the optical dielectric function using Kane's theory.[6] This change in the dielectric function is integrated over the space-charge region to obtain an averaged change in the dielectric function $\langle \Delta\epsilon \rangle$; finally we calculate and compare the calculated change in reflectance[7,8] with experimentally obtained ER data in InSb and InAs.

In Sec. III a simple oscillator model is described which leads to a more physical understanding of the observed broadening and splitting in the ER structure. The conclusion is contained in the fourth section with a discussion of the most relevant physical parameters in the analysis and of

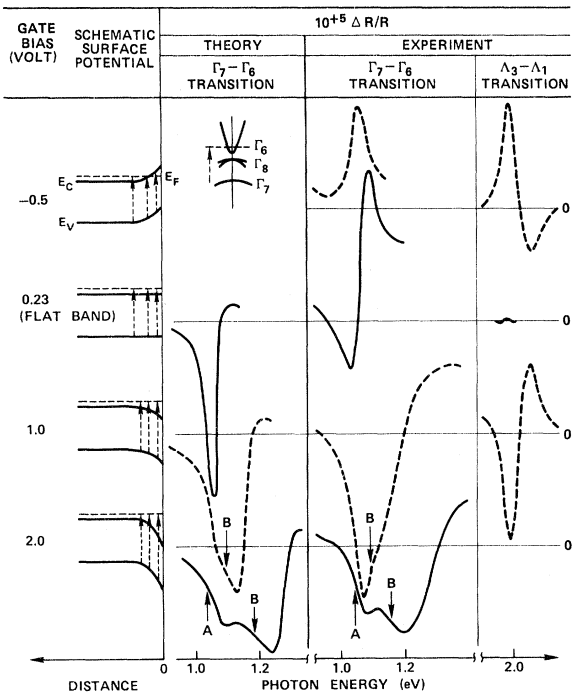

FIG. 1. Theoretical and experimental structures for electroreflectance $\Delta R/R$ in InSb as a function of dc bias and photon energy $\hbar\omega$. Two transitions are shown: The $\Gamma_7-\Gamma_6$ transition at $\vec{k}=0$ involving the initial spin-orbit-split valence-band states and the unoccupied final states in the conduction band, and the $\Lambda_3-\Lambda_1$ critical point transition along $\langle 111\rangle$. The surface potential as a function of bias and the associated photon transitions (dotted arrows) are shown schematically. The physical parameters for this material are given in Table I. The arrows A and B designate the values of the parameters E_0 and $E_0+V_S^*$ as described in the third section.

what can be learned about the fundamental parameters of degenerate materials from such ER experiments.

II. EXPERIMENTAL RESULTS AND COMPARISON WITH THEORY

A. InSb

Electroreflectance experiments were made using the metal-oxide-semiconductor (MOS) configuration.[9] Two structures were measured as a function of dc bias: the $\Gamma_7-\Gamma_6$ transition (the spin-orbit-split valence-band to lowest conduction-band transition) near 1 eV and the Λ_3-Λ_1 transition bridging the Fermi level. The latter structure was used primarily as a monitor of the surface potential and to determine surface flat-band condition.[10,11] The modulating voltage was a 0.5-V (peak to peak) 200-Hz square wave.

The two right-hand columns in Fig. 1 show the ER experimental results as a function of externally applied dc bias for the Γ and Λ transitions mentioned above. The surface condition for a given bias is shown schematically in the first column. The theoretically calculated line shapes for the normalized change in reflectance $\Delta R/R$, using the band-population mechanism outlined below, are shown in the second column.

The procedure used in calculating $\Delta R/R$ (column 2 of Fig. 1) is essentially given in Ref. 4. Basically, the application of a bias in the space-charge region of a semiconductor and the subsequent accumulation of carriers result in the lowering of the band structure relative to the Fermi level and thus a decrease in the availability of unoccupied final states. The onset of absorption is therefore shifted to higher frequencies as the bias is increased and this is schematically indicated in column 1 of Fig. 1; in general, the light samples the entire space-charge region. Since the band structure is significantly nonparabolic and since the potential in the space-charge region departs significantly from the predictions of linear screening, we had to modify the method of Ref. 4 according to the prescriptions given in the Appendices.

The determination of the bulk Fermi level E_F is the single most important parameter in determining the spectral position of the ER structure in degenerate semiconductors. Since E_F in degenerate materials is above the minimum of the conduction band $E_c(\vec{k})$, it is imperative to consider the nonparabolicity of E_c when calculating E_F. For InSb we used the Kane[6] approximation (Appendix A) to obtain $E_c(\vec{k})$. E_F was then calculated from the experimentally determined Hall carrier density n_H by an iterative process [Eq. (A1)]. At 78 °K, $n_H=6\times10^{16}$ cm^{-3} which yields the value $E_F=0.03$ eV for the InSb material used. Table I gives all the other pertinent physical parameters for InSb used in these calculations. In addition, the total carrier concentration was calculated to be 4×10^{16} cm^{-3}, considerably different from the Hall measurement.

Since in ER the light probes the spatially varying band population in the space-charge region, we calculated the potential distribution $V(z)$ near the surface by solving Poisson's relation for the degenerate semiconductor (Appendix B). In fact, the real parameter of interest in these calculations is the surface potential V_s because it directly relates to the experimental gate bias voltage V_G in the MOS configuration via Eq. (C8). V_s is a measure of the maximum population or rise of E_F relative to the conduction band under an accumulation condition. The (V_G-V_{FB})-vs-V_s relation is plotted in Fig. 2 for various values of the oxide capacitance per unit area C_0 for the degenerate InSb of

TABLE I. Physical parameters of InSb used in calculating the theoretical $\Delta R/R$ in Fig. 1.

Parameter		Value	Reference
Hall-effect conc.	n_H	6×10^{16} cm^{-3}	Hall measurement at 80 °K
Fermi level	E_F	0.03 eV	Calculated from Eqs. (A1–(A7) for nonparabolic bands
Lowest energy gap $\Gamma_8-\Gamma_6$	E_g	0.228 eV	Magnetoreflectance at 80 °K [a]
Energy gap $\Gamma_7-\Gamma_6$	E_g'	1.0 eV	Electroreflectance at 80 °K, in this paper
Spin-orbit split $\Gamma_7-\Gamma_8$	Δ_0	0.772 eV	Difference $(E_g'-E_g)$
Cyclotron-resonance effective mass	m_n	$0.012m_e$	Ref. 23 [a]
Valence-band effective mass	m_v^*	$0.11m_e$	Ref. 23 [a]
Screening length	λ_s	198 Å	Calculated from Eq. (B6)
Refractive index	n	4.15	b
Extinction coeff.	k	0.3	b
Static diel. const.	κ_s	17.8	a

[a] M. Neuberger, *Handbook of Electronic Materials: III-V Semiconducting Compounds* (Plenum, New York, 1971), Vol. 2.

[b] B. O. Seraphin and H. E. Bennett, in *Semiconductors and Semimetals*, edited by R. K. Willardson and A. C. Beer (Academic, New York, 1967), Vol. 3, pp. 499–543.

interest. These results were obtained numerically from Eqs. (B4) and (C8) and include the full nonparabolic bands and nonlinear screening treatment described in Appendix A. For comparison, the dotted curves show the results for the linear screening, nonparabolic bands, and nonlinear screening, parabolic band approximations.

In Fig. 2 the experimental V_s is still indeterminate unless the oxide capacitance and the flat-band voltage are known. Since critical-point transitions bridging the Fermi level (not affected by band population) show a null in ER for flat-band condition[10] at the fundamental frequency of modulation, we were able to determine V_{FB} quite accurately by monitoring the $\Lambda_3-\Lambda_1$ ER transition near 2 eV. Flat band occurred for $V_G=+0.23$ V for the sample of Fig. 1 (V_{FB} is sample and temperature dependent). The oxide capacitance was obtained from the oxide thickness of the Al_2O_3 and its value is given in the figure caption. Using these experimentally determined parameters we obtained $V_s=0, 0.065, 0.135$ V for the bias voltages $V_G=0.23$, 1.0, 2.0 V, respectively. The depth of modulation 0.5 V corresponds to a $\Delta V_s\simeq0.03$ V.

The final step in our calculation was the determination of the change in the complex dielectric function $\Delta\epsilon(\omega,z)$, its average $\langle\Delta\epsilon(\omega)\rangle$, and the relative change in the reflectivity $\Delta R/R$ by the procedure outlined in Appendix C. The only adjustable parameter in this calculation was the spin-orbit-split energy Δ_0.

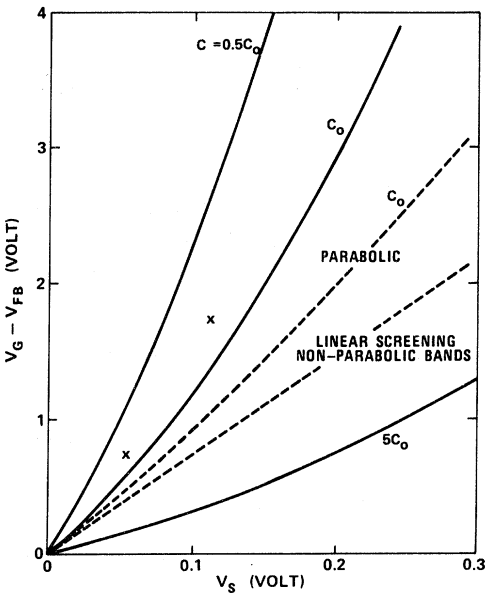

FIG. 2. Difference between the gate (V_G) and the flat-band (V_{FB}) voltage as a function of surface potential (V_s) as calculated from (B1), (B4), and (C8) using the nonparabolic band structure of InSb. The results for nonlinear screening, parabolic bands, and for nonparabolic bands, linear screening are shown by the dotted lines. C_0 is the experimentally measured oxide capacitance per unit area having the value 8.5×10^4 statfarad/cm^2. The X marks are experimentally intuited values of V_s vs V_G as determined from the A, B arrows of Fig. 1 (experimental) by the method described in Sec. III.

At this point we would like to emphasize that the nonparabolicity of the conduction band manifests itself essentially only through the calculated value of the surface potential as a function of gate bias, where it is a big effect (Fig. 2); the use of the nonparabolic band structure in the joint density of states [Eq. (C6)] or in the variation of the matrix element (C7) has little effect on our calculated $\Delta R/R$ although Kane[6] demonstrated that its use is necessary for both in the analysis of the fundamental absorption edge. In addition, the calculated $\Delta R/R$ was also relatively insensitive to the value of the (linear) screening length used in $V(z)$; the latter quantity is itself extremely insensitive to carrier concentration ($\lambda_s \propto n^{-1/6}$ for parabolic bands). As has been observed previously,[12] it is only necessary to accurately describe the field near the surface and approximately describe its decay into the bulk. We, therefore, feel justified in using linear screening to describe the decay of the potential into the bulk, $V(z) = V_s e^{-z/\lambda_s}$, although we must use nonlinear screening to determine an accurate value of V_s (as can also be seen from Fig. 2). We did not have to perform a self-consistent calculation[13] because of the relatively high carrier density ($r_s \lesssim 0.2$).

From Fig. 1 the following observations emerge: For increasing positive bias (accumulation condition), and thus increasing band population within the space-charge region, the spectral positions of $\Delta R/R$ (theory) and $\Delta R/R$ (experiment) are in good agreement. This agreement is good only if E_F and V_s are properly determined. Indeed, the agreement deteriorates for larger biases if the parabolic band approximation is assumed in the calculation. The inflection point of the $\Delta R/R$ structure on the low-energy "trailing" side is relatively insensitive to dc bias whereas that on the high-energy "leading" side of this structure is very bias dependent. Calculations show that this "trailing" edge is dependent on the bulk Fermi level and represents the onset of transitions from the valence band to the lowest unpopulated states in the conduction band (see the schematic band picture in Fig. 1.).

We find both experimentally and theoretically that there is a substantial broadening of the $\Delta R/R$ structure with increasing positive bias. This broadening represents the convoluted nature of $\Delta R/R$. That is, the structure in $\Delta\epsilon_2(\hbar\omega, z)$ is produced by the derivative of the Fermi-Dirac factor in Eq. (C2). Therefore, at very low temperatures this structure corresponds to a superposition of δ functions with a range of center frequencies. The range of these center frequencies represents the span of band population from minimum (bulk) to maximum (surface). The center frequency in each case corresponds to the energy separation between valence band and Fermi level at a specific point within the space-charge region. Since light probes all of these levels we obtain the convoluted structure seen in $\Delta R/R$. The half width of the $\Delta R/R$ structure for the 2-V bias case is 0.23 eV for both theory and experiment. A good agreement is also seen for the 1-V bias case.

The nature of the splitting in the $\Delta R/R$ structure for biases larger than 1 V will become apparent in Sec. III. For now it is worth noting that this peak separation is about 0.12 eV in the experiment and about 0.15 eV in the theory. The size-ratio between these two peaks is the same for both theory and experiment.

For flat-band bias the Λ transition reaches a null, but the structure due to the Γ transition is unaffected. This is to be expected since the former transition has a critical-point origin whereas the latter is a result of band population and even at the flat-band position the relative separation between the Fermi level and the valence band is still being monitored. As the bias becomes more and more negative (see Fig. 1), the Fermi level with respect to the conduction band will move into the forbidden band near the surface. Now the conduction band states near $\vec{k} = 0$ (the critical point) will start contributing to the transition. The net result is a mixture of critical-point transition (near the surface) and band-population associated transitions[4] (in the bulk). Of course, a pure band-population model is then no longer valid in representing this case.

B. InAs

The experimental conditions for measuring ER in InAs were similar to those of InSb. We were unable, however, to obtain good nonconducting MOS devices with InAs and, in addition, our devices exhibited a certain hysteresis in that the spectra obtained depended somewhat on the past history of biasing, presumably because of the population and depopulation of "slow" surface states. Of necessity, then, our analysis of InAs ER spectra should be considered semiquantitative at best.

Our best measured sample was degenerate due to the large Hall concentration ($n_H = 1.3 \times 10^{18}$ cm^{-3}) and the Fermi level is expected to be high in the conduction band (see last paragraph, this section). As expected, no structure was observed at 0.4 eV, the 78 °K absorption edge of an intrinsic InAs. In the 0.6–1.2-eV spectral range two structures appear as shown in Fig. 3. The peak separation between these two structures was 0.38 eV regardless of dc bias. This splitting corresponds very closely to the spin-orbit-split energy of InAs, thus we assign these two structures to the $E_0(\Gamma_8 - \Gamma_6)$ and the

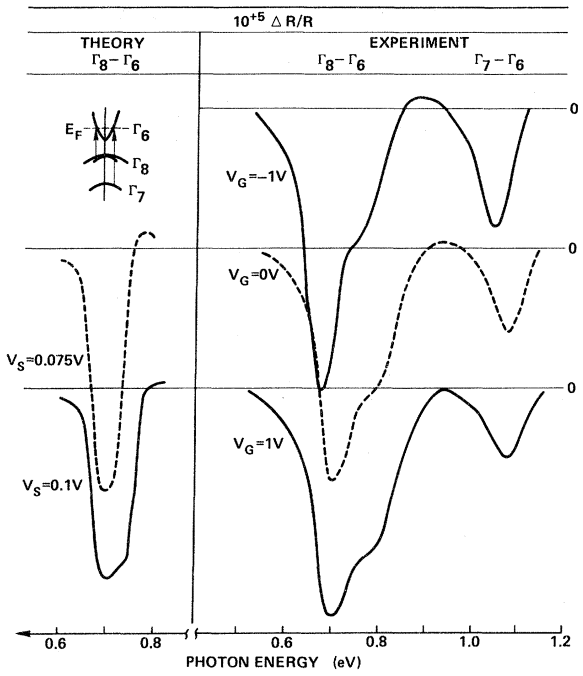

FIG. 3. Experimentally observed electroreflectance structure $\Delta R/R$ in InAs for the following two transitions: The $\Gamma_8-\Gamma_6$ transition (E_0) at $\vec{k}=0$ involving the top-most degenerate valence-band and the conduction-band states near the Fermi level, and the $\Gamma_7-\Gamma_6$ transition ($E_0-\Delta_0$) involving the spin-orbit-split valence band below it. These structures were measured at 78° K for various dc biases on a sample having the transparent metal-oxide-semiconductor configuration. Column 1 indicates the theoretically calculated $\Delta R/R$ curves as a function of surface potential V_s. The parabolic band approximation was used in determining the (V_G-V_{FB}) vs V_s relation.

$E_0+\Delta_0(\Gamma_7-\Gamma_6)$ structures in InAs, respectively. From this we conclude that the fundamental absorption edge was shifted to the blue 0.3 eV due to the Burstein-Moss shift. We were unable to bias the sample into depletion and thus we were unable to measure the flat-band voltage, as we did for InAs.

For InAs we make the following observations: The larger 0.7-eV peak in Fig. 3 shows the characteristic broadenings due to increased band population near the surface. The low-energy "trailing" edge is relatively insensitive to bias, whereas the high-energy "leading" edge shifts to the blue with increasing positive bias. Even for biases near MOS breakdown we were unable to achieve splitting in this structure. The $\Gamma_7-\Gamma_6$ structure also shows the broadening with bias, but the ER signal is too small to discern further details.

Theoretical calculations for $\Delta R/R$ were made to show the qualitative agreement between theory and experiment. Since the approximation $\Delta_0 \gg E_g$ does not apply for InAs and since we were unable to unambiguously identify the flat-band bias, we have analyzed the spectra in terms of an assumed parabolic conduction band. All parameters used are given in Table II. The Fermi level corresponding to a carrier density 1.3×10^{18} cm^{-3} in a parabolic band of mass $m^*=0.023\ m_e$ is $E_F=0.19$ eV. We have used the value 0.24 eV to bring our spectra into line with that observed. The discrepancy in Fermi levels is merely a reflection of probable error in the Hall measurement. As indicated previously, transitions to the bulk Fermi level occur at the low-energy side of our spectra. Notwithstanding the above comments, it is clear that the broadening-splitting effect observed in InSb is also observed here in InAs.

III. SIMPLE OSCILLATOR MODEL FOR $\Delta\epsilon$

In order to gain a better understanding of the unusual peak splitting and broadening behavior of our theoretical and experimental results, we wish to consider a simplified model based on Eq. (C2).

Because the derivative of the Fermi-Dirac factor in (C2) has a form very much like the imaginary part of a simple oscillator whose center frequency is shifted by bias (see, in particular, Fig. 2 of Ref. 4), we can approximately represent Eq. (C2) as (z negative in the material)

$$\Delta\epsilon(\hbar\omega,z)=f_0e^{+z/\lambda_s}/(\hbar\omega-E_0-V_s^*e^{+z/\lambda_s}+i\Gamma) \quad (1)$$

[the real and imaginary parts of Eq. (1) automatically obey the Kramers-Kronig relationships]. The oscillator strength f_0 is a smoothly varying function of $\hbar\omega$ and is proportional to $M_{cv}^2(\hbar\omega)\rho(\hbar\omega)$ (see Appendix C for definition). We will neglect its dependence on $\hbar\omega$ although this is not necessary. The exponential decay in the numerator arises from the decay of the ac modulation $\Delta V(z)=\Delta V_s e^{z/\lambda_s}$. Near the surface, the oscillator is centered about $E_0+V_s^*$, and this center frequency decays to E_0 deep in the bulk. If we assume parabolic bands, then V_s^* and E_0 are related to previously defined quantities by $E_0=E_g'+(m_c^*/\mu)E_F$ and $V_s^*=(m_c^*/\mu)V_s$, where m_c^* is the conduction-band mass and μ is the reduced mass. The broadening parameter Γ is proportional to temperature and represents the half width in the derivative of the Fermi-Dirac function ($\Gamma=1.76kT$).

Within this model, the convolution relation (C3) takes the form

$$\langle\Delta\epsilon(\hbar\omega)\rangle=-2iKf_0\int_{-\infty}^{0}\frac{dz'e^{-2iKz'+z'/\lambda_s}}{[\hbar\omega-E_0-V_s^*e^{+z'/\lambda_s}+i\Gamma]}. \quad (2)$$

Letting $x=e^{+z/\lambda_s}$ and $\xi=-2iK\lambda_s$, the above relation can be rewritten

TABLE II. Physical parameters of InAs used in calculating the theoretical $\Delta R/R$ in Fig. 3.

Parameter		Value	Reference
Hall-effect concentration	n_H	1.3×10^{18} cm^{-3}	Supplied by manufacturer [a]
Fermi level	E_F	0.24 eV	Chosen for agreement with experiment, present work
Lowest energy gap $\Gamma_8-\Gamma_6$	E_g	0.41 eV	Magnetoreflectance [b]
Spin-orbit split $\Gamma_7-\Gamma_8$	Δ_0	0.38 eV	Magnetoreflectance [b]
Energy gap $\Gamma_7-\Gamma_6$	E_g'	0.79 eV	$E_g+\Delta_0$
Cyclotron-resonance effective mass	m_c	$0.023m_e$	b
Valence-band effective mass	m_v	$0.41m_e$	b
Screening length	λ_s	100 Å	Calculated from Eq. (B7) for a parabolic band
Refractive index	n	3.51	c
Extinction coeff.	k	0.05	c
Static diel. const.	κ_s	14.5	b

[a] Metal specialties, Fairfield, Conn. 06430.
[b] See Table I, footnote a.
[c] See Table I, footnote b.

$$\langle\Delta\epsilon(\hbar\omega)\rangle = \xi f_0 \int_0^1 \frac{dx\, x^{\xi}}{\hbar\omega - E_0 - V_s^* x + i\Gamma}\,. \tag{3}$$

The integral above can be expressed in terms of Gauss's hypergeometric function,[14] given below, but it has a more elegant representation in terms of R_{-1}, Carlson's Dirichlet average.[15] The following, then, are equivalent representations of $\langle\Delta\epsilon\rangle$:

$$\langle\Delta\epsilon(\omega)\rangle = \frac{\xi}{\xi+1}\, f_0 R_{-1}(1, 1+\xi; \hbar\omega - E_0 + i\Gamma; \hbar\omega - E_0 - V_s^* + i\Gamma)\,, \tag{4a}$$

$$\langle\Delta\epsilon(\omega)\rangle = \frac{\xi f_0}{\xi+1}\, \frac{1}{\hbar\omega - E_0 + i\Gamma}\, {}_2F_1\left(1, 1+\xi; 2+\xi; \frac{V_s^*}{\hbar\omega - E_0 + i\Gamma}\right), \tag{4b}$$

$$\langle\Delta\epsilon(\omega)\rangle = \frac{\xi}{\xi+1}\, \frac{f_0}{\hbar\omega - E_0 - V_s^* + i\Gamma}\, {}_2F_1\left(1, 1; 2+\xi; \frac{-V_s^*}{\hbar\omega - E_0 - V_s^* + i\Gamma}\right). \tag{4c}$$

In addition, the function R_t has the interesting symmetry relation

$$R_t(a, b; x, y) = R_t(b, a; y, x)\,. \tag{5}$$

Equations (4a)–(4c) are suggestive that $\Delta R/R$ will show structure at the two frequencies $\hbar\omega \approx E_0$, which does not change with bias, and $\hbar\omega = E_0 + V_s^*$ which shifts monotonically to the blue with increasing accumulation bias. Both statements are true for $V_s = 0$ (flat band) which gives simply

$$\langle\Delta\epsilon(\hbar\omega)\rangle = \frac{\xi f_0}{\xi+1}\, \frac{1}{\hbar\omega - E_0 + i\Gamma} \quad (V_s \equiv 0)\,. \tag{6}$$

For $V_s \neq 0$, consider the identity[14,16]

$${}_2F_1(a, b; c; z) = \frac{\Gamma(c)\Gamma(b-a)}{\Gamma(b)\Gamma(c-a)}\, (-z)^{-a}\, {}_2F_1\left(a, 1+a-c; 1+a-b; \frac{1}{z}\right) + \frac{\Gamma(c)\Gamma(a-b)}{\Gamma(a)\Gamma(c-b)}\, (-z)^{-b}\, {}_2F_1\left(b, 1+b-c; 1+b-a; \frac{1}{z}\right). \tag{7}$$

Substituting (4b) into (7), we find the new identity

$$\langle\Delta\epsilon(\hbar\omega)\rangle = \frac{-f_0}{V_s^*}\, {}_2F_1\left(1, -\xi; 1-\xi; \frac{\hbar\omega - E_0 + i\Gamma}{V_s^*}\right) + \frac{\pi\xi f_0}{\sin(\pi\xi) V_s^*} \left(\frac{\hbar\omega - E_0 + i\Gamma}{-V_s^*}\right)^{\xi}. \tag{8}$$

For very low temperatures ($\Gamma \ll V_s^*$, as occurs in the two larger biases of Fig. 1), we find

$$\lim_{\hbar\omega \to E_0} \langle \Delta\epsilon(\hbar\omega)\rangle \to \frac{-f_0}{V_s^*} \tag{9}$$

because ${}_2F_1(a, b; c; 0) \equiv 1$ and $\mathrm{Re}(\xi) > 0$. Furthermore, because ${}_2F_1$ is a holomorphic function of z (cut from $+1$ to ∞), we see from Eq. (8) that some nth-order derivative of $\langle \Delta\epsilon \rangle$ with respect to ω will tend to diverge as $\hbar\omega \to E_0$ (if $\Gamma \ll V_s^*$). In our particular case of InSb, the parameters of Table I give $\xi \approx 0.1 - i$; Eq. (8) predicts that the first derivative of $\Delta R/R$ vs ω will tend to diverge at E_0. Although our calculated $\Delta R/R$ vs $\hbar\omega$ depends strongly on the nonparabolicity of the band structure through V_s vs V_G (Fig. 2), the nonparabolicity is otherwise relatively unimportant in Eq. (C2) because the Γ_7 band is relatively flat. Accordingly, we make the parabolic approximation for E_0 (see above), and this value is indicated by the arrow A in the theoretical curves of Fig. 1. As predicted, the (low frequency) inflection point for all curves with $V_s \gg kT$ lies very near E_0, independent of bias. We therefore deduce the value E_0 from the experimental curves of Fig. 1; this coincides well with E_0 calculated from Table I because we had adjusted Δ_0 to bring the theory into agreement with experiment.

In order to show that there is structure at $\hbar\omega = E_0 + V_s^*$, we consider the identity[14,16]

$$\begin{aligned} {}_2F_1(a, b; a+b; z) = {} & \frac{\Gamma(a+b)}{\Gamma(a)\Gamma(b)} \sum_{n=0}^{\infty} \frac{(a)_n (b)_n}{(n!)^2} \left[2\Psi(n+1) - \Psi(a+n) - \Psi(b+n)\right](1-z)^n \\ & - \ln(1-z) \frac{\Gamma(a+b)}{\Gamma(a)\Gamma(b)} \sum_{n=0}^{\infty} \frac{(a)_n (b)_n}{(n!)^2} (1-z)^n . \end{aligned} \tag{10}$$

For $\hbar\omega \approx E_0 + V_s^*$, Eq. (4b) substituted in (10) gives

$$\langle \Delta\epsilon(\hbar\omega)\rangle \approx \frac{-\xi f_0}{V_s^* + i\Gamma} \left[\Psi(1+\xi) - \Psi(1) + \ln\left(\frac{\hbar\omega - E_0 - V_s^* + i\Gamma}{V_s^* + i\Gamma}\right)\right], \tag{11}$$

and we see that there is predicted to be a weak, logarithmic divergence in $\Delta R/R$ as $\hbar\omega \to E_0 + V_s^*$ (at low temperatures) with a stronger divergence in the slope. Accordingly, we have calculated the values of $E_0 + V_s^*$ for each bias, using Fig. 2 and Table I, with $E_0 + V_s^*$ indicated by arrow B in the second column of Fig. 1. Note that $V_s^* \equiv 0$ at flat band. As expected, the positions of $E_0 + V_s^*$ correlate well with the positions of the inflection points of the split-off peak. Once again we deduce the approximate values of $E_0 + V_s^*$ in our experimental curves.

At this point we have deduced experimental values of V_s^* for each value of the bias V_G. V_s^* is related to V_s, the surface potential, through a knowledge of the band structure. In particular $V_s^* = (m_c^*/\mu)V_s$ for parabolic bands; if the initial state is essentially flat, $V_s^* \equiv V_s$, independent of the conduction-band structure. In Fig. 2, the × marks indicate the values of V_s that we have deduced from the position of the arrows in the experimental curves of Fig. 1, plotted as a function of gate bias. We see that agreement with the calculated curve V_s vs V_G for nonlinear screening due to nonparabolic bands is excellent. Indeed, when we either used linear screening or made the approximation of parabolic bands in Fig. 2, our theoretical results for Fig. 1 were found to shift much more strongly to the blue as the bias was increased. We conclude that this method provides a relatively simple optical means of monitoring the surface potential of an accumulation-biased degenerate semiconductor in an MOS configuration.

Physically, structure occurs at $E_0 + V_s^*$ since the ac modulation is strongest at the surface. Structure occurs at E_0 because this is the frequency at which the bulk contributes. The total width of the observed structure increases with V_s^*. For large values of V_s^* there will be sufficient spectral resolution in the experiment to observe the above described divergences at $\hbar\omega = E_0$ and $E_0 + V_s^*$. Contributions from oscillators centered at intermediate frequencies [see Eq. (3)] integrate out in a manner reminiscent of the theory of the de Haas–van Alphen effect[17] wherein only extremal orbits contribute to the magnetization, although the mathematics are quite different in the two cases.

The relative strengths of the structures at E_0 and $E_0 + V_s^*$ are governed by the parameter

$$\begin{aligned} \xi &= -2iK\lambda_s = 2(\omega/c)(k - in)\lambda_s \\ &= 2\lambda_s(1/\delta - 2\pi i/\lambda_D), \end{aligned}$$

where δ and λ_D are, respectively, the penetration depth and wavelength of the light in the dielectric (semiconductor). This parameter determines whether the decay of the bias e^{z/λ_s} occurs over a shorter or longer distance than the variation of the

photon field e^{-2iKz}. (The factor of 2 arises because the light penetrates a distance z, is partially reflected, and must propagate back out.) The limiting cases are

Metallic: $\xi \approx 0$. This implies $\lambda_s \ll \frac{1}{2}\delta$ *and* $\lambda_s \ll \lambda_D/4\pi$. Equation (3) yields

$$\lim_{\xi\to 0}\langle\Delta\epsilon(\omega)\rangle = \xi(f_0/V_s^*)[\ln(\hbar\omega - E_0 + i\Gamma) - \ln(\hbar\omega - E_0 - V_s^* + i\Gamma)] \quad (12)$$

[the convergence $x^t \to 1$ is not uniform, but Eq. (12) is true nonetheless]. In this case the potential decays within a distance over which the photon field varies hardly at all. Although there is structure of equal strength at E_0 and at $E_0 + V_s^*$, both are weak because of the prefactor. In addition, V_s itself is small, as can be seen from the linearized version of Eq. (C8) given in Ref. 4.

$$V_G - V_{FB} = [1 + (\kappa_s/\kappa_{0x})(t_{0x}/\lambda_s)]V_s . \quad (13)$$

These considerations merely point up the obvious: It is difficult (but not impossible[18]) to do ER on ordinary metals.

Weakly metallic: $|\xi| \to \infty$. This can occur *either* if $\lambda_s \gg \frac{1}{2}\delta$ *or* if $\lambda_s \gg \lambda_D/4\pi$. In either case the probing photon sees an effectively constant $\Delta\epsilon(z)$. Substituting the series expansion[14] for ${}_2F_1$ into Eq. (4c) we obtain

$$\lim_{|\xi|\to\infty}\langle\Delta\epsilon(\omega)\rangle = \frac{f_0}{\hbar\omega - E_0 - V_s^* + iF} . \quad (14)$$

In Eq. (14) although the structure at $E_0 + V_s^*$ is "large," the structure at $\hbar\omega \approx E_0$ is negligible because the photon is not able to effectively sample the bulk of the dielectric. This is obvious if $\lambda_s \gg \frac{1}{2}\delta$; it is also true if $\lambda_s \gg \lambda_D/4\pi$ even if $\lambda_s \ll \frac{1}{2}\delta$.

The optimal condition for seeing *appreciable* structure both at E_0 and at $E_0 + V_s^*$ is evidently $|\xi| \approx 1$. The parameters for InSb listed in Table I give $\xi(\text{InSb}) \approx 0.1 - 1.0i$ and, as seen in Fig. 1, the two structures are of comparable and appreciable strength. On the other hand, the InAs parameters give $\xi(\text{InAs}) \approx 0.1 - 0.2i$; as discussed above, it is difficult to get a large value of the potential at the surface; consequently there is little of the splitting effect in InAs. Finally, in Ref. 4 the parameters used for PbSe give $\xi(\text{PbSe}) \approx 0.8 - 2.4i$, and we may expect Eq. (14) to be approximately correct. Indeed, each value of $E_0 + V_s^*$ occurs exactly at the (single) maximum in the calculated $\Delta R/R$ vs ω of Fig. 5, Ref. 4. In addition, there is very weak structure at $\hbar\omega \approx E_0$ for all values of the bias which did not show on the scale of Fig. 5, Ref. 4.

The three materials InAs, InSb, and PbSe seem, then, to more or less span the range from small $|\xi|$ to large $|\xi|$. The parameter ξ does depend on the doping through λ_s, but only weakly.

IV. SUMMARY AND CONCLUSIONS

Spatially varying band population within the space-charge region of a semiconductor gives rise to unusual ER structure which broadens, shifts, and in some cases splits as a function of increased surface charge accumulation. In an effort to explain these phenomena in terms of a band-population model, we have considered explicitly the band nonparabolicity and nonlinear screening in the calculation of $\Delta R/R$. These calculations not only helped to explain the observed broadening and splitting of the $\Gamma_7 - \Gamma_6$ ER structure in InSb, but also pointed the way towards a more intuitive approach to the problem. By representing $\Delta\epsilon$ by a simple oscillator model whose center frequency shifts with local bias, we were able to explain the salient features in the experimental ER results without recourse to sophisticated numerical calculations. By considering the limiting cases in this model, we were able to establish criteria in determining the presence or absence of strong broadening and splitting in terms of the screening length, the wavelength, and penetration depth of light in the medium. Furthermore, these criteria enabled us to deduce from the ER measurements the position of the Fermi level in the bulk and the effective surface potential as a function of external gate bias.

ACKNOWLEDGMENTS

We would like to acknowledge many fruitful discussions concerning the ${}_2F_1$ function with B. C. Carlson, and we are most grateful for technical assistance from J. Kinoshita.

APPENDIX A: FERMI LEVEL AND CARRIER DENSITY IN DEGENERATE SEMICONDUCTORS WITH NONPARABOLIC BANDS

For highly doped narrow-gap semiconductors it is reasonable to assume that all localized impurity levels are screened out; i.e., we are on the metallic side of the Mott transition. Under this assumption, the electronic band structure for the doped material is the same as that for the intrinsic material except that the excess carriers reside solely in the conduction or valence band (as the case may be).

In principle, the knowledge of the nonparabolic band structure enables one to calculate the total electron or hole concentration from a known Fermi level and vice versa. Unfortunately, however, we do not *a priori* know either.

The most direct method of obtaining the bulk Fermi level (E_F) of a degenerate semiconductor is to measure the Hall coefficient. At sufficiently low temperatures ($E_F/kT \gg 1$) the Hall carrier

density n_H is given by[19]

$$n_H(E_F) = \tfrac{1}{3} m^*(E_F) v^2(E_F) \rho(E_F) , \tag{A1}$$

where the effective mass m^*, the Fermi velocity v, and the density of states ρ can be obtained from the usual energy-band relations

$$1/m^* = \frac{1}{\hbar^2} \frac{d^2E}{dk^2} , \tag{A2a}$$

$$v = \frac{1}{\hbar} \frac{dE}{dk} , \tag{A2b}$$

$$\rho = \frac{k^2}{\pi^2} \frac{dk}{dE} . \tag{A2c}$$

For a simple parabolic band (m^* const), the Hall carrier density reduces to the well-known relation

$$n_H = (1/3\pi^2)(2m^*E_F/\hbar^2)^{3/2} = n_{\text{tot}} . \tag{A3}$$

In general, however, the total number of carriers, given by

$$n_{\text{tot}} = \int_0^{E_F} \rho(E)\, dE \tag{A4}$$

is not equal to (A1).

Hence, knowing the band relation $E(\vec{k})$ of a material, E_F can be calculated from (A1)–(A2) by using an iterative process. For example, for semiconductors having spherical nonparabolic bands and large spin-orbit splitting (spin-orbit splitting Δ_0 much greater than lowest gap energy E_g) the conduction-band relation can be written with the aid of Kane's approximation[6] as

$$E_c(k) = (\hbar^2k^2/2m_e) + \tfrac{1}{2}\eta^{1/2} - \tfrac{1}{2}E_g , \tag{A5}$$

$$\eta = E_g^2 + \tfrac{8}{3} P^2k^2 , \tag{A6}$$

where m_e is the electron mass and P the matrix element which is related to the experimental cyclotron resonance mass m_n by[20]

$$P^2 = \tfrac{3}{4}(m_e - m_n)E_g\hbar^2/m_em_n . \tag{A7}$$

In summary, we then use Eqs. (A1)–(A7) and the values in Table I to determine E_F iteratively from a knowledge of the Hall carrier density.

APPENDIX B: SCREENING-LENGTH AND SURFACE-CHARGE RELATIONS IN A DEGENERATE SEMICONDUCTOR

In deriving the screening length for a degenerate semiconductor it is convenient to use Ehrenreich's expression[20] for the carrier density n in the conduction band

$$\begin{aligned} n &= (1/\pi^2)(2m_nkT/\hbar^2)^{3/2}[F_{1/2}(x) + \beta^*(\tfrac{5}{2} - 5\mu)F_{3/2}(x) \\ &\quad + \beta^{*2}(1 - \tfrac{21}{2}\mu)F_{5/2}(x) \\ &\quad - 4\mu\beta^{*3}F_{7/2}(x)] \\ &= N_c \sum_j C_j F_j(x) = N_c \rho(x), \quad j = \tfrac{1}{2}, \tfrac{3}{2}, \tfrac{5}{2}, \tfrac{7}{2} , \end{aligned} \tag{B1}$$

where $x = E_F/kT$, $\beta^* = kT/E_g$, $\mu = m_n/m_e$, and $F_j(x)$ is the Fermi-Dirac integral

$$F_j(x) = \int_0^\infty \frac{dt\, t^j}{\exp(t - x) + 1} . \tag{B2}$$

Equation (B1) is valid under Kane's approximation ($\Delta \gg E_g$) and the assumption that $\mu \ll 1$.

The surface charge Q_s can be obtained by integrating the Poisson relation[21]

$$\frac{d^2V}{dz^2} = \frac{4\pi e}{\kappa_s}[n(z) - n_0] , \tag{B3}$$

where κ_s is the static dielectric constant, V the potential, and z the distance into the material. In terms of the density of states and the unitless potential $u = eV/kT$ within the space charge region, Q_s takes the form

$$\begin{aligned} Q_s &= \frac{\kappa_s kT}{4\pi e}\left(\frac{du}{dz}\right)_s \\ &= \left(\frac{2\kappa_s N_c kT}{\pi}\right)^{1/2}\left(\int_{u_s}^0 du[\rho(x+u) - \rho(x)]\right) . \end{aligned} \tag{B4}$$

Equation (B4) can be solved analytically if $x > 20$ (very heavy doping) by using the Sommerfeld approximation[22] $F_j(x) = (j+1)^{-1}x^{j+1}$. Also, for small u, we can expand in u and keep linear terms. In the latter case Eq. (B3) reduces to the form

$$\frac{d^2u}{dz^2} = \frac{1}{\lambda_s^2} u , \tag{B5}$$

where now by using Eq. (B1) a screening length λ_s can be defined by

$$\begin{aligned} \frac{1}{\lambda_s^2} &= \frac{4\pi e^2 N_c}{\kappa_s kT} \frac{d}{dx} \rho(x) \\ &= \frac{4\pi e^2 N_c}{\kappa_s kT} \sum_j jC_j F_{j-1}(x) . \end{aligned} \tag{B6}$$

For $kT/E_F \ll 1$ the above relation reduces to the usual Thomas-Fermi screening length[19] λ_{TF}

$$1/\lambda_{TF}^2 = 4\pi e^2 \rho(E_F) . \tag{B7}$$

APPENDIX C: PROCEDURE FOR CALCULATING THE RELATIVE CHANGE IN THE REFLECTIVITY $\Delta R/R$ IN DEGENERATE SEMICONDUCTORS

For an n-type degenerate semiconductor, the contribution to the imaginary part of the dielectric function ϵ_2 for the electronic transitions under study will have the form

$$\epsilon_2(\hbar\omega) = M_{cv}^2 \rho_{cv}(\hbar\omega)(1 - f_c) , \tag{C1}$$

where ρ_{cv} is the interband density of state, M_{cv} the matrix element for the transition, $\hbar\omega$ the photon energy, and f_c the Fermi-Dirac distribution func-

tion.

In modulation experiments (e.g., electroreflectance) of heavily doped semiconductors, the quasi-equilibrium position of the Fermi level relative to the conduction band near the surface can be shifted by an external bias potential V_G. The induced change in ϵ_2 by V_G within the space charge region is

$$\Delta\epsilon_2(\hbar\omega, z) = +M_{cv}^2 \rho_{cv} \frac{df_c}{dV} \Delta V(z) = \epsilon_2(\hbar\omega) \frac{d}{dV} (\exp\{-[E_c(\hbar\omega) - E_F - eV(z)]/kT\} + 1)^{-1} \Delta V(z), \quad \text{(C2)}$$

and $\Delta\epsilon_1(\hbar\omega, z)$ is calculated from the Kramers-Kronig integration[4] of (C2). The convoluted form of this change $\langle\Delta\epsilon(\hbar\omega)\rangle$ can be calculated from the Aspnes-Frova relation[7]

$$\langle\Delta\epsilon(\hbar\omega)\rangle = -2iK \int_{z\to-\infty}^{0} dz' e^{-2iKz'} \Delta\epsilon(\hbar\omega, z'), \quad \text{(C3)}$$

where K is the complex refractive index $(\omega/c)(n + ik)$. Finally, $\Delta R/R$ is determined from[8]

$$\Delta R/R = \mathrm{Re}[-(2n_a n_s D)^{-1} \langle\Delta\epsilon\rangle], \quad \text{(C4)}$$

where n_a and n_s are refractive indices of the ambient and substrate material; the parameter D completely describes the effect of surface layers on the substrate (the metal electrode and the oxide) and is related to the generalized Seraphin coefficients α and β by[8]

$$\alpha - i\beta = -(2n_a n_s D)^{-1}. \quad \text{(C5)}$$

We calculated the interband density of states $(k^2/\pi^2)(dk/d\hbar\omega)$ using the Kane theory.[6] For each $\hbar\omega$ the value of k is obtained from (A5) and

$$\hbar\omega = E_c(k) - E_v(k)$$
$$= E_g' + \hbar^2 k^2/2m_c + \tfrac{1}{2}\eta^{1/2}/2 - \tfrac{1}{2}E_g + \hbar^2 k^2/2|m_v^*|. \quad \text{(C6)}$$

E_g' above represents the energy difference between the conduction band and some valence band with effective mass m_v^* at $\vec{k} = 0$ other than the uppermost valence band. Equation (C6) can be inverted analytically for $k(\omega)$.

The matrix element for the transition is calculated using the expression

$$M_{cv}^2 = (2m_e^2 P^2/3\hbar^2)[(a_c c_v + c_c a_v)^2 + (a_c b_v - b_c a_v)^2], \quad \text{(C7)}$$

where the coefficients a, b, and c as a function of k are given in Ref. 6.

The remaining task is to calculate the potential distribution within the space charge region of the degenerate material for a given external bias. This will allow the determination of band population at each point z within the surface region. The form $V(z) = V_s e^{-z/\lambda_s}$ is a very good approximation for the potential distribution provided V_s and λ_s can be determined accurately.[12] The linear screening length is calculated from (B6) once E_F is known. The surface potential V_s follows from the experimental sample configuration. In electroreflectance experiments using the metal-oxide-semiconductor configuration, V_s can be obtained from[21]

$$V_G - V_{FB} = V_s - Q_s/C_0, \quad \text{(C8)}$$

where C_0 is the oxide capacitance and Q_s is given by Eq. (B4). V_{FB} is that gate voltage which produces a vanishing electric field throughout the semiconductor up to the interface; it depends on the true surface charge density and the metal-semiconductor work-function difference.[21] V_{FB} is determined experimentally from the so-called "flatband" condition[10] where the $\Lambda_3 - \Lambda_1$ electroreflectance signal disappears. Figure 2 shows the (V_G, V_s) relation for near-degenerate InSb for various oxide capacitances. These results include the full nonparabolic treatment as described in Appendix B. The parabolic-band-approximation curve is shown for comparison. $\Delta\epsilon_2(\hbar\omega, z)$ and $\Delta\epsilon_1(\hbar\omega, z)$ can now be calculated numerically and $\Delta R/R$ determined from (C4).

*Present address: Physics Dept., Northeastern University, Boston, Mass. 02115.

[1]E. Burstein, Phys. Rev. 93, 632 (1954).
[2]T. S. Moss, Proc. Phys. Soc. Lond. B 76, 775 (1954).
[3]R. Glosser and B. O. Seraphin, Phys. Rev. 187, 1021 (1969).
[4]N. Bottka and D. L. Johnson, Phys. Rev. B 11, 2969 (1975).
[5]N. Bottka, R. Glosser, and J. Kinoshita, Bull. Am. Phys. Soc. 2, No. 3 (1975).
[6]E. O. Kane, J. Phys. Chem. Solids 1, 249 (1957).
[7]D. E. Aspnes and A. Frova, Solid State Commun. 7, 155 (1969).
[8]D. E. Aspnes, J. Opt. Soc. Am. 63, 1380 (1973).
[9]J. E. Fischer, Rev. Sci. Instrum. 42, 872 (1971).
[10]B. O. Seraphin, R. B. Hess, and N. Bottka, J. Appl. Phys. 36, 2242 (1965).
[11]F. Holtz, Phys. Status Solidi A 21, 469 (1974).
[12]N. Bottka, J. Appl. Phys. 44, 5626 (1973).
[13]G. A. Baraff and J. A. Appelbaum, Phys. Rev. B 5, 475

(1972).
[14]National Bureau of Standards, in *Handbook of Mathematical Functions*, edited by M. Abramowitz and I. A. Stegun, Natl. Bur. Stands. Applied Mathematical Series, (U.S. GPO, Washington, D. C., 1964), Vol. 55.
[15]B. C. Carlson, Stud. Appl. Math. 6, 30 (1970).
[16]N. N. Lebedev, *Special Functions and Their Applications*, translated and edited by R. A. Silverman (Prentice-Hall, Englewood Cliffs, N. J., 1965). The properties of the hypergeometric function are derived most simply here, as are the restrictions on the parameters.
[17]I. M. Lifschitz and A. M. Kosevich, Zh. Eksp. Teor. Fiz. 29, 730 (1956) [Sov. Phys.-JETP 2, 636 (1956)]. Extremal orbits dominate because integrals of the form $\int \exp[if(z)]g(z)dz$ are evaluated in the method of stationary phase by expanding $f(z)$ about a stationary point where $df/dz=0$. In Eq. (2), $f(z)\propto z$ has no stationary point.
[18]T. E. Furtak and D. W. Lynch, Phys. Rev. Lett. 35, 960 (1975).
[19]J. M. Ziman, *Electrons and Phonons, The Theory of Transport Phenomena in Solids* (Clarendon, Oxford, England, 1967), p. 487.
[20]H. Ehrenreich, J. Phys. Chem. Solids 2, 131 (1957).
[21]A. S. Grove, B. E. Deal, E. H. Snow, and C. T. Sak, Solid-State Electron 8, 145 (1964).
[22]J. S. Blackmore, in *Semiconductor Statistics*, International Series of Monographs on Semiconductors, edited by Heinz K. Henisch (Pergamon, New York, 1962), Vol. 3, p. 357.